Engineering of Hole Transporting Interface by Incorporating the Atomic-Precision Ag_6 Nanoclusters for High-Efficiency Blue Perovskite Light-Emitting Diodes

Fujun Zhang[a,§], Yanbo Gao[a,§,], Po Lu[a], Yuan Zhong[a], Yue Liu[a], Xinyu Bao[a], Zehua, Xu[a], Min Lu[a], Yanjie Wu[a], Ping Chen[a], Junhua Hu[b], Yu Zhang[a], Zhennan, Wu[a,]*, Hongwei Song[a,]*, and Xue Bai[a,]**

[a] State Key Laboratory of Integrated Optoelectronics, College of Electronic Science and Engineering, Jilin University, Qianjin Street, Changchun, 130012, China.

[b] Key Laboratory of Materials Physics of Ministry of Education Department of Physics and Engineering, Zhengzhou University, Zhengzhou, 450052, China.

§ These authors contributed equally to this work.

* Corresponding author.

E-mail: gaoyanbo@jlu.edu.cn (Y. Gao); wuzn@jlu.edu.cn (Z. Wu); songhw@jlu.edu.cn (H. Song); baix@jlu.edu.cn (X. Bai)

Materials and methods

Materials

Dimethyl sulfoxide (DMSO, 99.99%) and chlorobenzene (CB, 99.99%) were purchased from Advanced Election Technology Co., Ltd. PEDOT: PSS (AI 4083) aqueous solution, 2,2',2"-(1,3,5-Benzinetriyl)-tris(1-phenyl-1-H-benzimidazole) (TPBi, 99.9%), Lead(II) bromide ($PbBr_2$, 99.99%), Phenylbutylamine bromide (PBABr, 99.9%), poly [9,9-dioctylfluoreneco-N-[4-(3-methylpropyl)]diphenylamine] (TFB), Poly(9-vinylcarbazole) (PVK), and (8-Quinolinolato)lithium (Liq, 99.9%) were purchased from Xi'an Polymer Light Technology Corp. (S)-4-Phenylthiazolidine-2-thione (99%), silver nitrate (99%), NaSCN (98%), ZnBr (98%), dodecane (99%), CH3COOAg (99%), 2-hexyldecanoic acid (99%), dimethylacet-amide (DMAc, 99%), acetonitrile (CH_3CN, 99%), acetic acid (99%), and oleylamine (80%) were purchased from Shanghai Aladdin Biochemical Technology Co., Ltd. All reagents were used as received without further purification.

Device fabrication

The indium tin oxide (ITO)-coated glass substrates were sequentially washed with water, ethanol, and acetone in sequence for 20 min and treated with O_3 plasma for 15 min. The PEDOT: PSS films were fabricated on the washed ITO by spin coating the PEDOT: PSS aqueous solution at the speed of 3000 rpm for 30 s and baked at 150 °C for 30 min in ambient air. Then the TFB (in m-xylene, 8 mg ml^{-1}) was spin-coated on the top of PEDOT: PSS films at 2000 rpm for 60 s, followed by annealing on a hot plate at 120 °C for 15 min in the glove box. The PVK (in CB, 10 mg ml^{-1}) or the modified PVK films were fabricated by spin-coated on the top of TFB films at 2000 rpm for 60 s, followed by annealing on a hot plate at 120 °C for 15 min in the glove box.

The Ag_6 nanoclusters were prepared by dissolving (S)-4-Phenylthiazolidine-2-thione (0.1 mmol) and silver nitrate (0.1 mmol) into a mixed solvent of DMAc/CH_3CN (3:1), which evaporated slowly in darkness at room temperature for 48 hours. Then the Ag nanocluster naturally dries and dissolves in CB with stirring for more than 4 hours to accelerate dissolution. The doping concentration ratio of Ag_6 NCs is based on the concentration of PVK. The Ag nanoparticles were synthesized based on the method reported by Long Lin et al..[1]

The perovskite solution was fabricated by mixing the $PbBr_2$ (0.1 mmol), CsBr (0.1 mmol), PBABr (0.1 mmol), NaSCN (0.005 mmol), $ZnBr_2$ (0.005 mmol) and crown (0.005 mmol) in 1mL of DMSO. Then the perovskite solution was spin-coated on the top of PVK films at 300 rpm for 5 s, 500rpm for 5 s, and 3000 rpm for 120 s, and after spin coating for 70 s, 100 μL ethyl acetate was immediately dropped onto the above film to template the crystallization of the perovskite crystals, followed by annealing on a hot plate at 55 °C for 10 min. Finally, TPBi, Liq, and Al electrode layers were sequentially deposited by thermal evaporation (1×10^{-5} Torr).

Characterizations

Absorption and PL spectra were measured on Shimadzu UV-1900i spectrometer and Hitachi F-4700 spectrometer, respectively. TEM images were obtained on a JEM-2100F. SEM images and elemental mapping were collected on a JSM-7900F instrument. X-ray photoelectron spectroscopy (XPS) and ultraviolet photoelectron spectroscopy (UPS) were measured on an ESCALAB250 spectrometer. The roughness and the KPFM of the film were characterized by atomic force microscopy (AFM, Dimension Fastscan Bio, CA). The diffraction of X-rays (XRD) was conducted by using the grazing incidence (GI) mode in Rigaku Smartlab 9 kw. Cyclic voltammetry (CV) experiments were measured using the three-electrode system in chromatographic grade acetonitrile, and Tetrabutylammonium hexafluorophosphate (0.1 mol/L) was used as a supporting electrolyte. The three-electrode cell contained an Ag wire reference electrode (Chenhua, China), a Pt (platinum) wire counter electrode (Chenhua, China) and a glass-carbon working electrode (3 mm diameter, Chenhua, China). The surface area of the glass-carbon working electrode was polished with 0.3 and 0.5 aluminas (Chenhua, China), and then followed by ultrasonic cleaning three times in deionized water. All the cyclic voltammetry data were calibrated by ferrocene.[2] Time-resolved PL measurements were performed with a time-correlated single-photon counting system of the FLS920P Edinburgh spectrometer. The absolute PLQYs of the quasi-2D perovskite films were measured on a fluorescence spectrometer (FLS920P, Edinburgh Instruments) equipped with an integrating sphere. The current density- voltage and luminance- voltage curves and the EL spectra of the LEDs were collected on a Keithley

2400 source meter and an integrating sphere (OceanOptics) coupled to a spectrophotometer in the darkroom, respectively.

Density functional theory

The structure of Ag_6PL_6 was taken from the crystal structure in the literature, and the structure of PVK was constructed in which n = 5. The dipoles (i.e., Ag_6PL_6 mixed with PVK) formed between Ag_6PL_6 and PVK was also constructed. Then the geometry optimizations of Ag_6PL_6, PVK, and PVK with Ag_6 NCs were carried out by density functional theory (DFT) calculations using the Dmol[3] module[3] in the Materials Studio software package.[4] The Perdew-Burke-Ernzerh of (PBE)[5] modification of the generalized gradient approximation (GGA)[6] with the Grimme[7,8] custom method for DFT-D correction together with the doubled numerical basis set (DN) was used. The core electrons were treated by all electrons, and a global orbital cutoff of 3.4 Å and a Fermi smearing of 0.005 Ha were used for the optimizations. The convergence criteria include a self-consistent field (SCF) tolerance of 1.0×10^{-4} Ha per atom, a maximum force tolerance of 0.004 Ha $Å^{-1}$, an energy tolerance of 2.0×10^{-5} Ha per atom, and a maximum displacement tolerance of 0.005 Å were employed.

To understand the intermolecular interaction between Ag_6PL_6 and PVK in the dipoles (Ag_6PL_6 and PVK), the noncovalent interaction (NCI)[9,10] analysis was used to elaborate the intermolecular interaction appearing between Ag_6PL_6 and PVK which was plotted by the Multiwfn software.[11]

Calculations of the surface potential from the KPFM

The contact potential difference (CPD) between the tip and sample can be obtained by KPFM from equation (1)[12]:

$$\Delta CPD = (\emptyset_{tip} - \emptyset_{sample})/e \quad (1)$$

where e is the electronic charge and the $\emptyset_{tip}$ and ϕ_{sample} are the work function of the tip and the film, respectively.

Calculations of the electrical conductivity (σ) from the current-voltage curves of capacitor-like devices

The electrical conductivity (σ) of the PVK and modified PVK films can be investigated by the current-voltage curves of capacitor-like devices from equation (2)[13]:

$$\sigma = \frac{LI}{AV} \tag{2}$$

where the L, I, A, and V are the thickness of the films, current, device area, and voltage, respectively.

Calculations of the hole mobility from the space-charge-limited-current region (SCLC)

The hole mobility can be calculated by the current density-voltage curves of the single carrier device from equation (3)[13]:

$$J = \frac{9\varepsilon\varepsilon_0\mu V^2}{8L^3} \tag{3}$$

where the L is the thickness of the film, $\mu, J, \varepsilon, \varepsilon_0$ and V are the mobility, current density, relative dielectric constant, vacuum permittivity, and voltage, respectively.

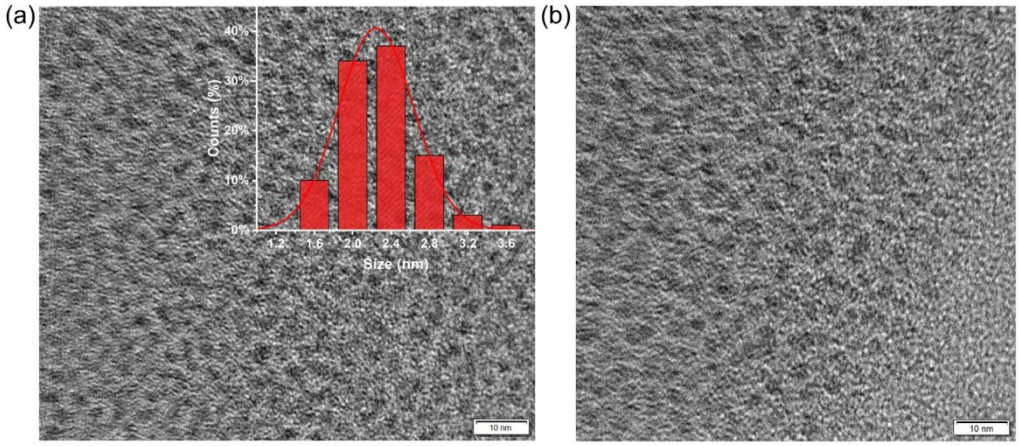

Figure S1. The TEM of the Ag_6 NCs in CB, and the inset image show the size distribution.

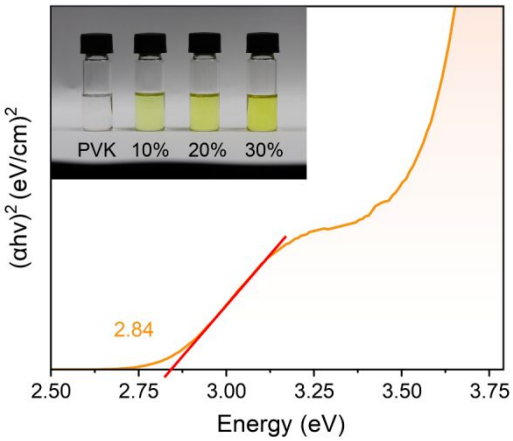

Figure S2. The Tauc-plot of the Ag_6 NCs and the inset picture is the PVK with the different concentrations of the Ag_6 NCs in CB solvent.

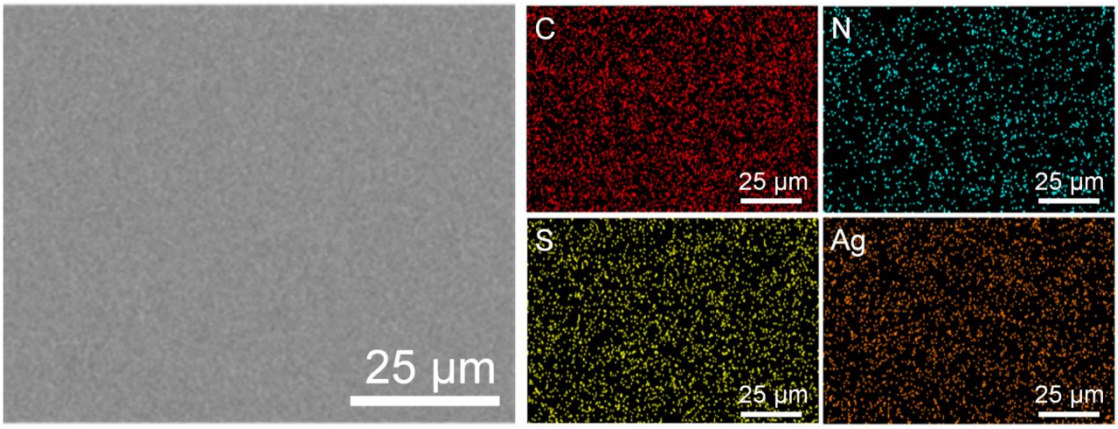

Figure S3. The SEM and mapping images of the PVK film with the 20% Ag_6 NCs doped.

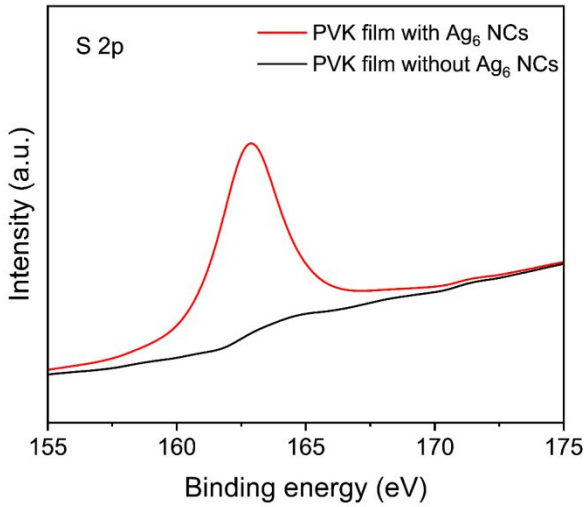

Figure S4. The XPS spectra of the PVK films with and without Ag_6 NCs.

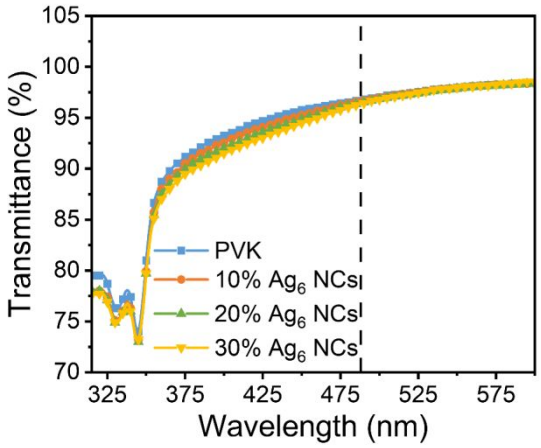

Figure S5. The transmissivity of the PVK and the different concentrations of Ag_6 NCs doping into PVK films.

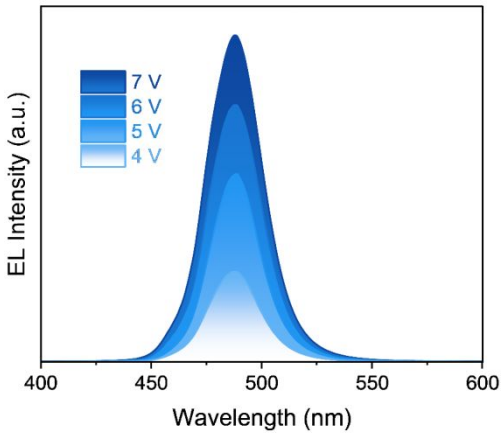

Figure S6. The evolution of EL spectra under increasing bias voltage from 4 V to 7 V of the control device.

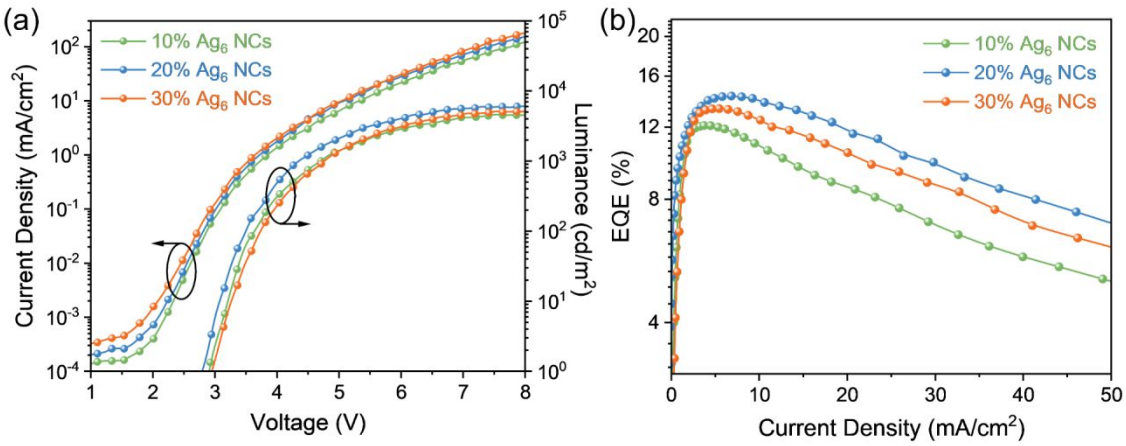

Figure S7. The J-V-L curves (a) and the EQE-J curves (b) of the device with different concentrations of Ag_6 NCs doping into PVK as the HTL.

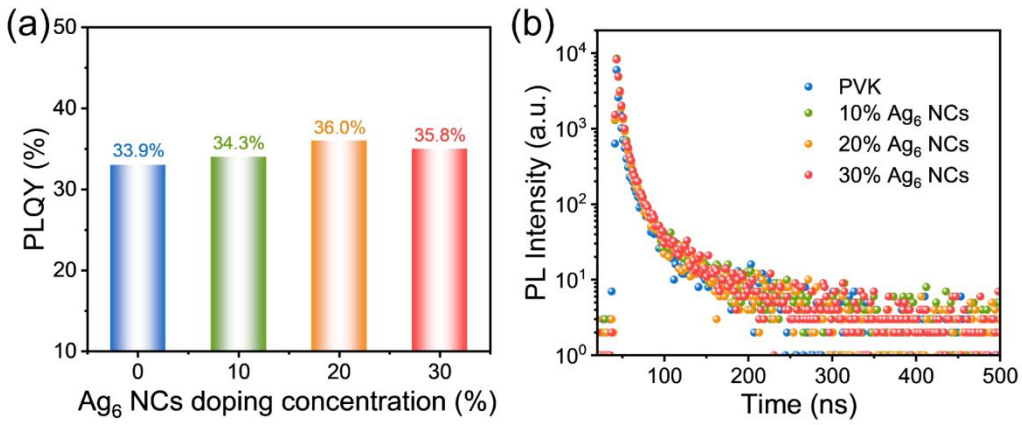

Figure S8. The PLQY (a) and TRPL (b) of the perovskite films on the PVK films with different concentrations of Ag_6 NCs doping. The PLQY of the perovskite films on PVK and 10%, 20%, and 30% of the Ag_6 NCs doped PVK films is 33.9%, 34.3%, 36%, and 35.8%, and the corresponding average lifetimes are 7.3, 8.6, 9.3, and 9.1 ns, respectively.

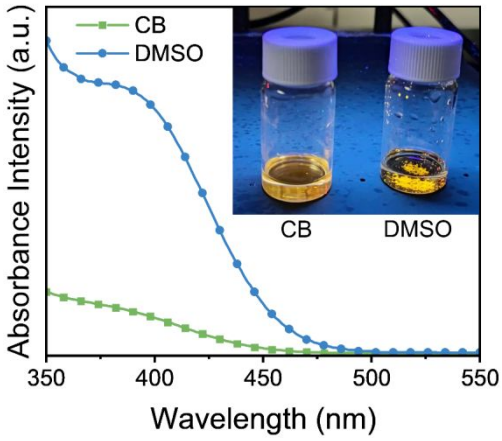

Figure S9. The absorption spectra of the Ag_6 NCs in different solvents (CB and DMSO).

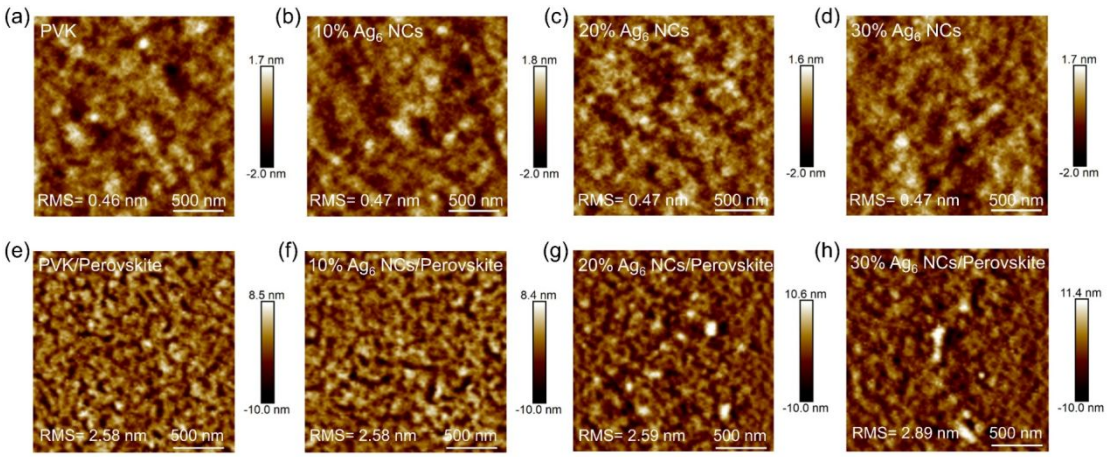

Figure S10. The AFM images of the 0- 30% Ag_6 NCs doping into PVK films (a-d) and the perovskite films on different HTLs (e-h).

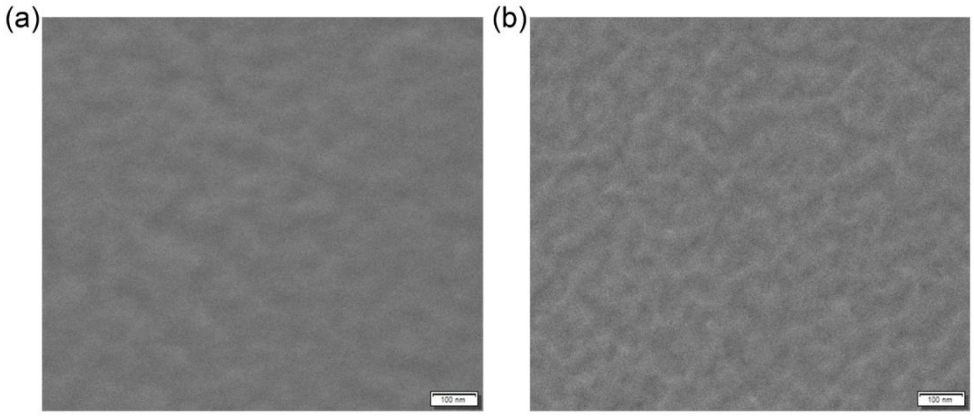

Figure S11. The SEM images of the perovskite on the PVK (a) and 30% Ag_6 NCs modified PVK (b).

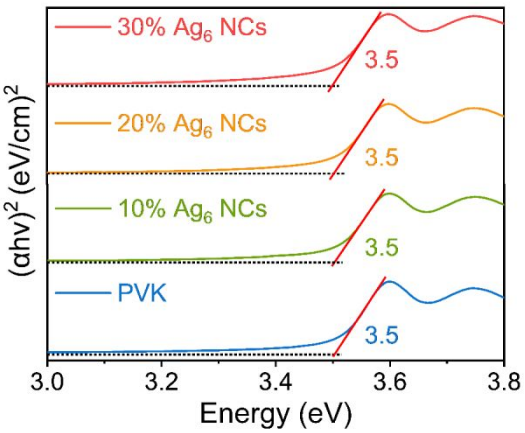

Figure S12. The Tauc-plots of the PVK and different concentrations of Ag_6 NCs doping into PVK films

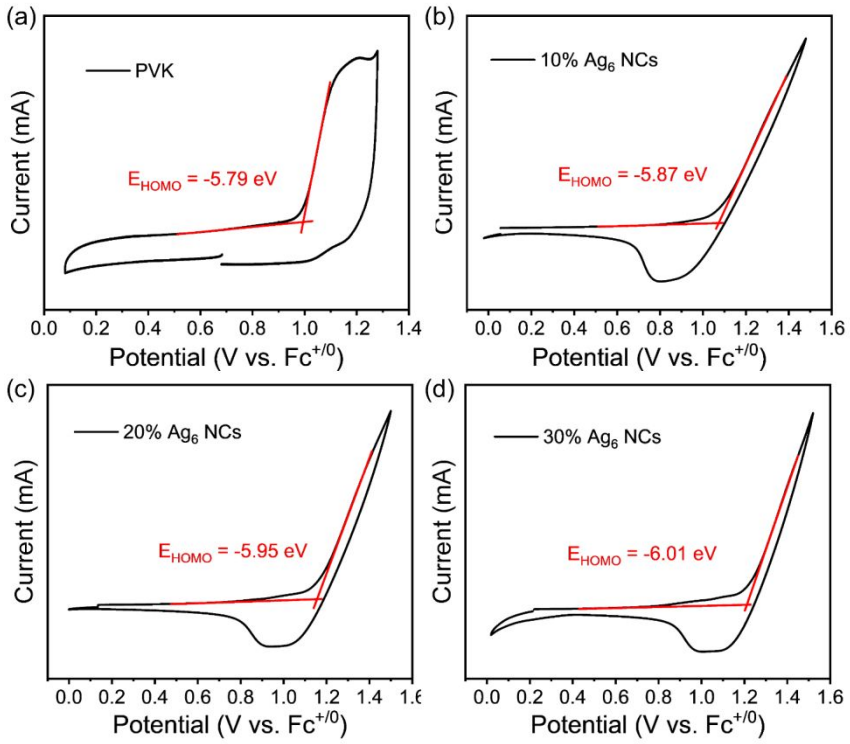

Figure R13. The CV curves of the PVK and PVK with different concentrations of Ag_6 NCs doped. The HOMO energy of the pure PVK, 10%, 20%, and 30% Ag_6 NCs doing into PVK samples are -5.79, -5.87, -5.95, and -6.01 eV, respectively.

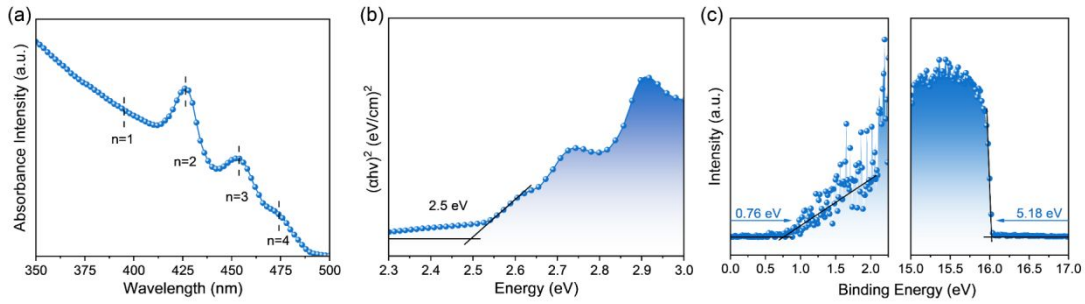

Figure S14. The absorbance intensity spectrum (a), Tauc-plot (c), and UPS spectra of the perovskite films (c).

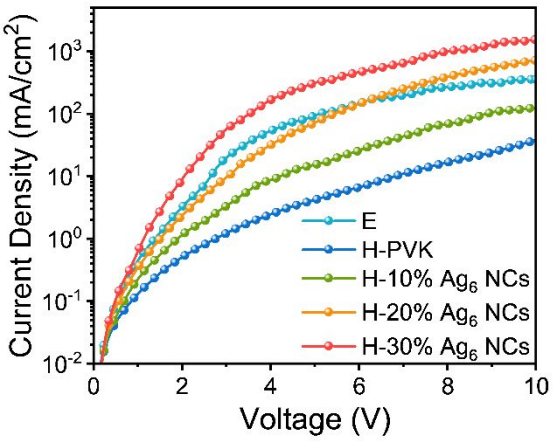

Figure S15. The J-V curves of the hole-only and electron-only devices with the structure of ITO/PEDOT: PSS/TFB/pure PVK and PVK with different concentrations of Ag_6 NCs doping/perovskite/4,4',4"-tris(carbazol-9-yl)-triphenylamine (TCTa)/MoO_3/Au (hole-only device) and ITO/ZnO/polyethyleneimine (PEI)/perovskite/TPBi/Liq/Al (electron-only device).

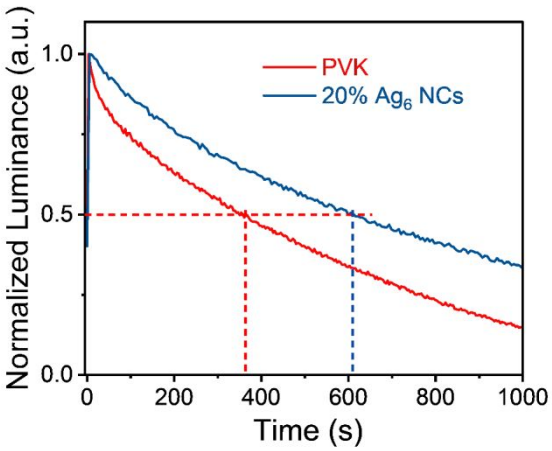

Figure S16. The operation stability of the control (PVK) and optimized devices (20% Ag_6 NCs).

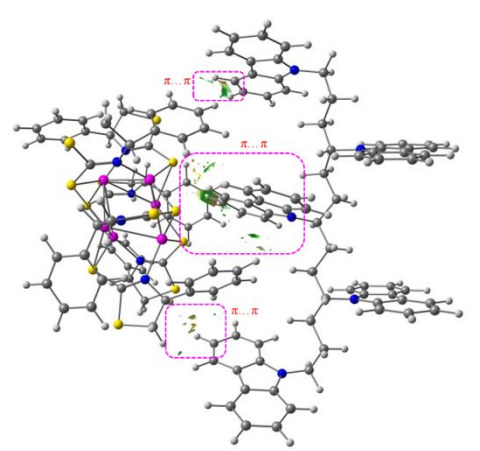

Figure S17. The non-covalent interaction (NCI) analyses of the dipoles (i.e., Ag_6 NCs and PVK), where the small green clouds were highlighted by the pink-dotted grids.

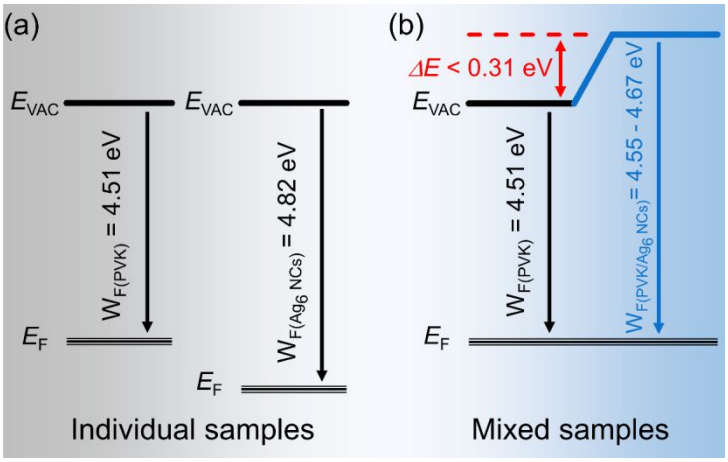

Figure S18. The mechanism of energy level alignment tuning from dipoles (i.e., Ag_6 NCs and PVK). The W_F difference between the Ag_6 NCs and PVK (a), the E_{vac} shift of the mixed samples.

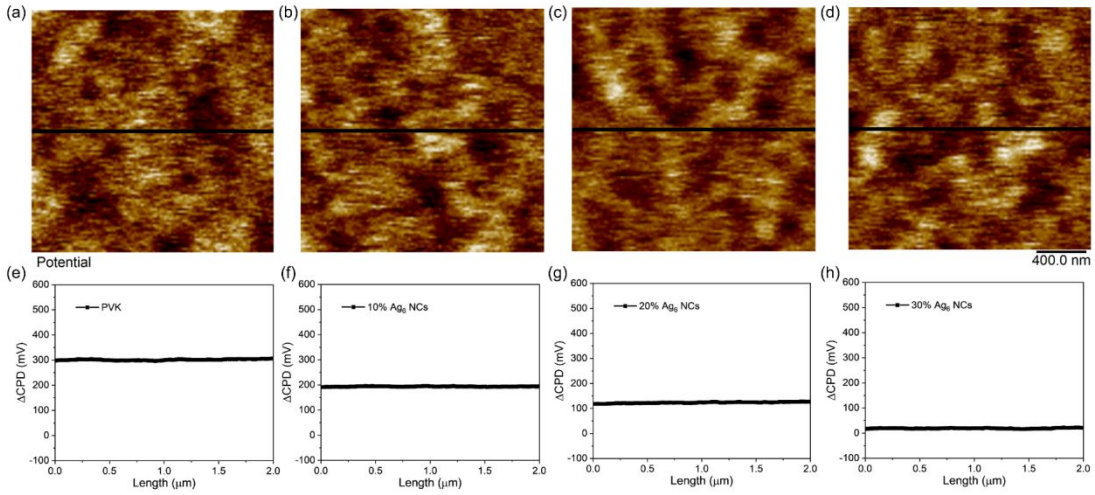

Figure S19. The surface potential images of PVK film and the 0- 30% Ag_6 NCs doping into PVK films (a-d). With the increased doping concentration of Ag_6 NCs, theΔCPD decreased from around 0.30 mV to ~ 0.03 mV.

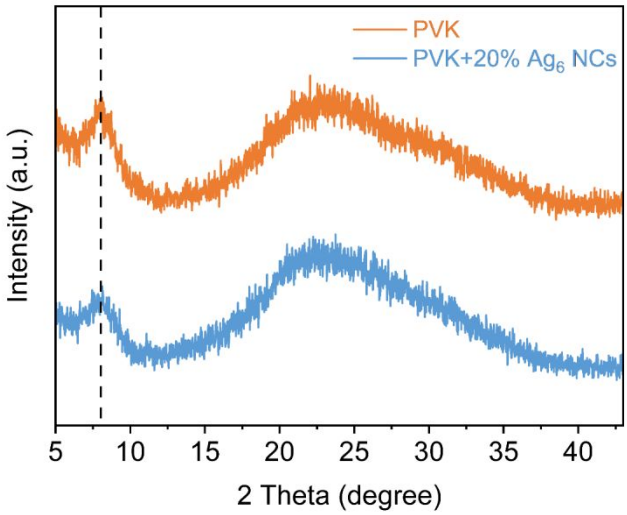

Figure S20. The GI-XRD of the PVK and 20%Ag_6 NCs modified PVK films.

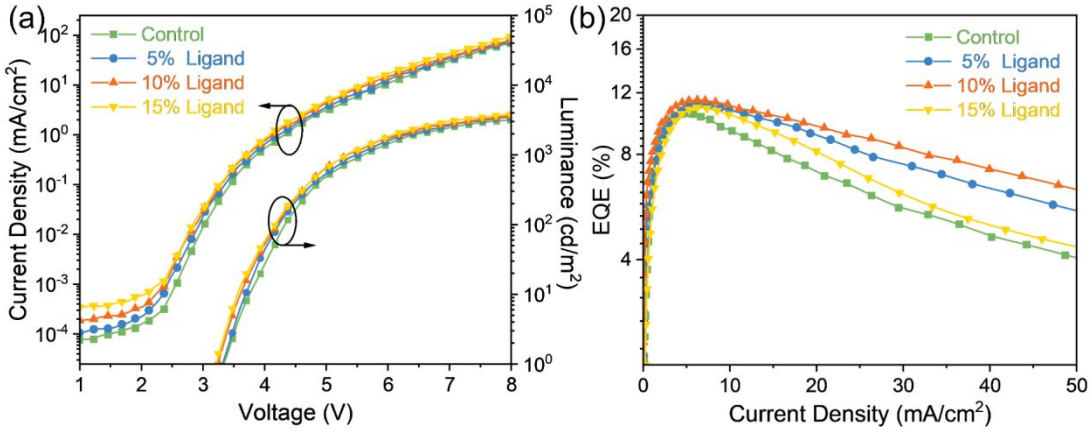

Figure S21. The J-V-L curves (a) and the EQE-J curves (b) of the device with different concentrations of ligands doping into PVK as the HTL.

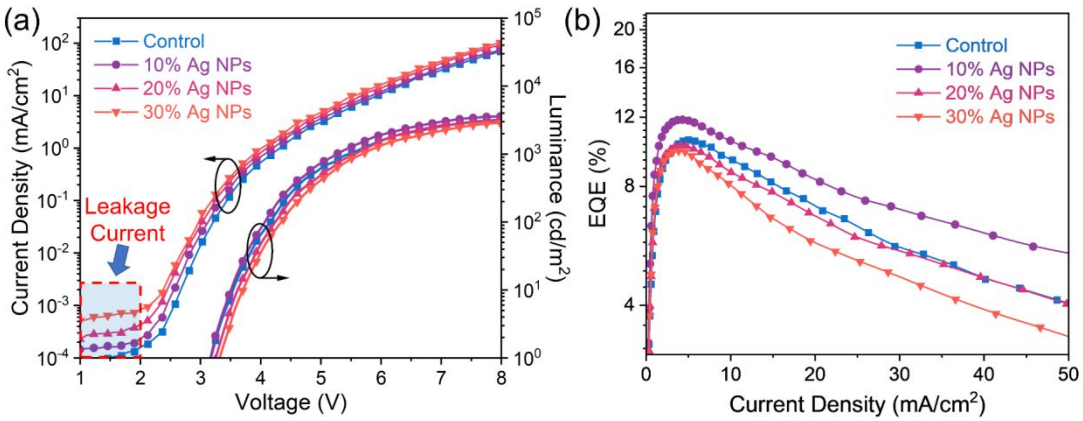

Figure S22. The J-V-L curves (a) and the EQE-J curves (b) of the device with different concentrations of Ag NPs doping into PVK as the HTL.

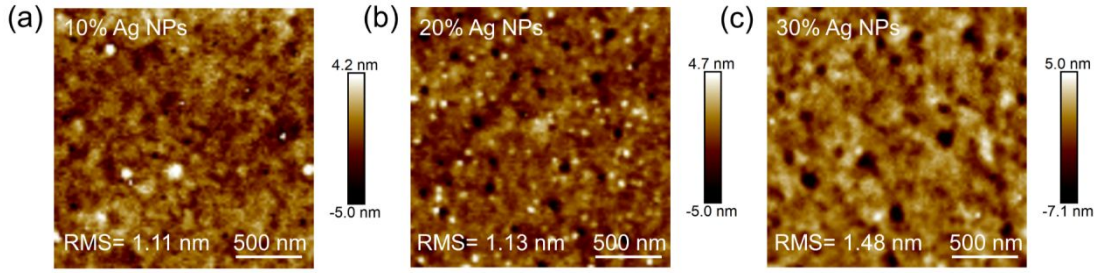

Figure S23. The AFM of the PVK with the 0- 30% Ag NPs modified films.

References

(1) Lin, L.; Chen, M.; Qin, H.; Peng, X. Ag Nanocrystals with Nearly Ideal Optical Quality: Synthesis, Growth Mechanism, and Characterizations. *J. Am. Chem. Soc.* **2018**, *140* (50), 17734–17742. https**:**//doi.org/10.1021/jacs.8b10793.

(2)Wang, Y.; Shen, R.; Wang, S.; Chen, Q.; Gu, C.; Zhang, W.; Yang, G.; Chen, Q.; Zhang, Y.-M.; Zhang, S. X.-A. A See-through Electrochromic Display via Dynamic Metal-Ligand Interactions. *Chem.* **2021**, *7* (5), 1308–1320. https://doi.org/10.1016/j.chempr.2021.02.005.

(3) Delley, B. From Molecules to Solids with the DMol(3) Approach. *J. Chem. Phys.* **2000**, *113* (18), 7756–7764. https://doi.org/10.1063/1.1316015.

(4)DMol3 Module, MS Modeling, Version 2.2, Accelrys Inc., San, Diego, CA, 2003.

(5) Perdew; Burke; Ernzerhof. Generalized Gradient Approximation Made Simple. *Phys Rev Lett* **1996**, *77* (18), 3865–3868. https://doi.org/10.1103/PhysRevLett.77.3865.

(6) Monkhorst, H. J.; Pack, J. D. Special Points for Brillouin-Zone Integrations. *Phys. Rev. B* **1976**, *13* (12), 5188–5192. https://doi.org/10.1103/PhysRevB.13.5188.

(7) Grimme, S. Semiempirical GGA-Type Density Functional Constructed with a Long-Range Dispersion Correction. *J. Comput. Chem.* **2006**, *27* (15), 1787–1799. https://doi.org/10.1002/jcc.20495.

(8) Grimme, S.; Antony, J.; Ehrlich, S.; Krieg, H. A Consistent and Accurate Ab Initio Parametrization of Density Functional Dispersion Correction (DFT-D) for the 94 Elements H-Pu. *J. Chem. Phys.* **2010**, *132* (15), 154104. https://doi.org/10.1063/1.3382344.

(9) Contreras-García, J.; Johnson, E. R.; Keinan, S.; Chaudret, R.; Piquemal, J.-P.; Beratan, D. N.; Yang, W. NCIPLOT: A Program for Plotting Noncovalent Interaction Regions. *J. Chem. Theory Comput*. **2011**, *7* (3), 625–632. https://doi.org/10.1021/ct100641a.

(10)Johnson, E. R.; Keinan, S.; Mori-Sánchez, P.; Contreras-García, J.; Cohen, A. J.; Yang, W. Revealing Noncovalent Interactions. *J. Am. Chem. Soc*. **2010**, *132* (18), 6498–6506. https://doi.org/10.1021/ja100936w.

(11)Lu, T.; Chen, F. Multiwfn: A Multifunctional Wavefunction Analyzer. *J. Comput. Chem.* **2012**, *33* (5), 580–592. https://doi.org/10.1002/jcc.22885.

(12)Gao, Y.; Wu, Y.; Liu, Y.; Lu, M.; Yang, L.; Wang, Y.; Yu, W. W.; Bai, X.; Zhang, Y.; Dai, Q. Interface and Grain Boundary Passivation for Efficient and Stable Perovskite Solar Cells: The Effect of Terminal Groups in Hydrophobic Fused Benzothiadiazole-Based Organic Semiconductors. *Nanoscale Horiz.* **2020**, *5* (12),

1574–1585. https://doi.org/10.1039/D0NH00374C

(13) Shen, X.; Zhang, X.; Wang, Z.; Gao, X.; Wang, Y.; Lu, P.; Bai, X.; Hu, J.; Shi, Z.; Yu, W. W.; Zhang, Y. Bright and Efficient Pure Red Perovskite Nanocrystals Light-Emitting Devices via In Situ Modification. *Adv. Funct. Mater.* **2022**, *32* (8), 2110048. https://doi.org/10.1002/adfm.202110048.